PREPUBLICACIONES DEL DEPARTAMENTO
DE MATEMÁTICA APLICADA
UNIVERSIDAD COMPLUTENSE DE MADRID
MA-UCM 2013-05

Mathematical modelling of the growth and coarsening of ice particles in the context of high pressure shift freezing processes

N. A. S. Smith, V. M. Burlakov and A. M. Ramos

Abril-2013

http://www.mat.ucm.es/deptos/ma
e-mail:matemática_aplicada@mat.ucm.es

Mathematical modelling of the growth and coarsening of ice particles in the context of high pressure shift freezing processes

N.A.S.Smith,[†] V. M. Burlakov,[‡] and Á. M. Ramos[*,†]

Universidad Complutense de Madrid, and Oxford University

E-mail: angel@mat.ucm.es

[*]To whom correspondence should be addressed

[†]Instituto de Matemática Interdisciplinar, Departamento de Matemática Aplicada, Facultad de Ciencias Matemáticas, Universidad Complutense de Madrid,, Plaza de Ciencias 3, 28040, Madrid, Spain.

[‡]Mathematical Institute, OCCAM, University of Oxford, 24-26 St Giles, Oxford OX1 3LB, UK.

Abstract

High Pressure Shift Freezing (HPSF) has been proven more beneficial for ice crystal size and shape than traditional (at atmospheric pressure) freezing.[1–3] A model for growth and coarsening of ice crystals inside a frozen food sample (either at atmospheric or high pressure) is developed and some numerical experiments are given, with which the model is validated by using experimental data. To the best of our knowledge this is the first model suited for freezing crystallisation in the context of High Pressure.

1 Motivation for studying growth and coarsening of ice particles

Recent advances in food preservation are related to development of the so-called High Pressure Shift Freezing (HPSF) method, which allows achieving a very quick and homogeneous decrease of the tissue temperature.[1–5] Such a shift in temperature quickly brings the water within the tissue well below its freezing point hence causing homogeneous nucleation of large number of very small ice particles.[1–5] Further growth of these particles decreases the freezing point of remaining water by increasing concentration of salts in it and finally stops the ice precipitation. Thus, the HPSF method allows avoiding formation of relatively large, tissue damaging ice crystals[6] during their relatively quick growth phase. These bigger crystals are generated due to much slower process of ripening when the mass of ice is transferred from smaller to bigger ice particles.[7–9]

The goal of this work is to develop a model to study the growth and coarsening of ice particles in a frozen food sample, and hence look at the temporal evolution of HPSF frozen ice crystals. This idea came from the work published by Fernández et al.[6], where the authors investigated if HPSF frozen systems follow the same ice recrystallisation kinetics as those conventionally frozen (at atmospheric conditions). A system which could hold HPSF frozen samples of suitable size for microscopic observation without their alteration was designed.[6] Then using direct microscopic examination at different temperatures, they could follow the evolution of ice crystals with time and

study the influence of the freezing method and storage temperature on recrystallisation. In Fernández et al.[6] a 1.86N NaCl solution was used as a food model sample. In this paper we use this model system to study theoretically and numerically the time evolution of ice particles. This evolution involves both growth and ripening processes described within the mean field approximation. The proposed approach is rather generic and remains valid for any type of freezing process provided that the particles have roughly spherical shape and are evenly distributed over the sample volume.

In Section 2 we describe how to calculate the melting temperature of salty water and show some expressions regarding the salt mass concentration and the volume concentration of dissolved ice. In Section 3 we present a model that accounts for the growth and ripening of ice crystals in this system by developing a theory somewhat similar to Ostwald ripening.[7–9] Our model predicts crystal size evolution with time, and also ice crystal size distribution. In Section 4 we describe the numerical simulations we have performed and in Section 5 we present the particular numerical experiments and results for salty water and ice-cream. In Section 6 we outline the conclusions.

2 Melting temperature of salty water

Consider a system consisting of salty water at an experimental temperature T_{exp} (K). If the temperature is low enough (below the melting point) the system has a potential to produce a certain amount of ice (which depends on the temperature[10]) via isothermal crystallisation. Let us assume that at time t_0 (s) the system has already produced part of this ice, which has precipitated in spherical particles of radii R_i (μm). It is also convenient to assume that all the ice which can potentially precipitate at a given temperature, is initially dissolved in salty water, i.e. we mark the corresponding fraction of water molecules as being dissolved ice molecules. Such representation allows introducing an effective excess concentration of water, which we will use to develop a theory somewhat similar to Ostwald ripening to account for both growth and coarsening of the pre-existing ice particles.

In the course of ice precipitation the salt concentration increases pushing the melting tempera-

ture T_{melt} down towards T_{exp}. Once the latter is reached the ice precipitation stops such that $T_{\text{melt}}(t)$ remains equal to T_{exp} for any $t \geq \bar{t}$. At times $t \geq \bar{t}$ some ice particles may still grow due to ripening process.

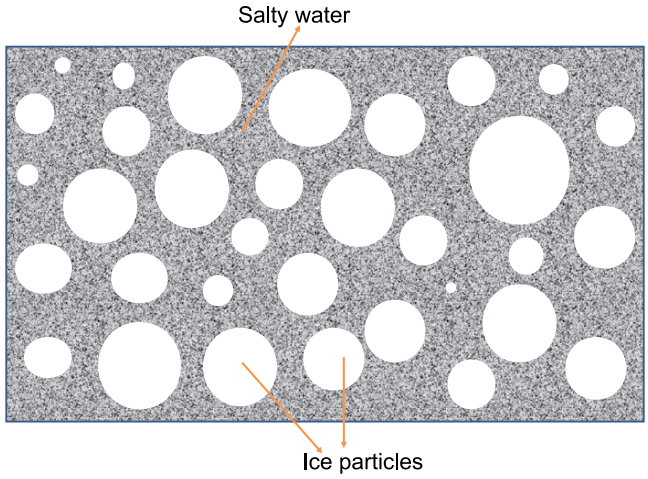

Figure 1: Salty water system configuraton.

Suppose that at time t the system is composed of salty water and spherical (for simplicity) precipitated ice particles of radii $R_i(t)$ as illustrated in Figure 1. The salt mass concentration in the system can be expressed as

$$x_s(t) = \frac{M_s}{V_{\text{s.water}} + V_{\text{ice}}(t)}, \tag{1}$$

where M_s (mg) is the total salt mass dissolved in water and non-precipitated dissolved ice, $V_{\text{s.water}}$ (μm^3) is the volume occupied by salty water that is not part of the non-precipitated ice dissolved in water, and $V_{\text{ice}}(t)$ (μm^3) is the volume occupied by the non-precipitated ice dissolved in water.

First we illustrate the dependence of the melting temperature upon the salt concentration. In thermodynamic equilibrium at melting temperature $T_{\text{melt}}(x_s)$ the chemical potentials of H_2O molecules in the non-precipitated ice (μ_{ice}) and in salty water ($\mu_{\text{s.water}}$) are equal.

For chemical potential of water molecules in ice particles we can neglect entropic contribution and write

$$\mu_{\text{ice}} = -\varepsilon_{\text{ice}} \tag{2}$$

which is constant for the range of temperatures and pressures under consideration, where ε_{ice} (eV per molecule) is the cohesive energy of H_2O molecules in ice.

For water molecules in salty water the chemical potential depends on x_s,[11] so we have that

$$\mu_{\text{s.water}}(x_s) = -\varepsilon_{\text{water}} - \beta x_s + kT \ln\left(\frac{n_{\text{water}}}{n_{\text{max}}}\right), \tag{3}$$

where $-\beta$ (eV μm^3 mg^{-1} per molecule) is the rate of change of $\mu_{\text{s.water}}$ with respect to x_s, $\varepsilon_{\text{water}}$ is the cohesive energies of H_2O molecules in pure water, k is the Boltzmann constant ($k \approx 1.3806488\text{x}10^{-23}$J K^{-1} = $8.6173324\text{x}10^{-5}$eV K^{-1}), $n_{\text{water}} = v_{\text{water}}^{-1}$ (molecules per μm^3) is the number concentration of H_2O molecules in water and n_{max} is the maximum number concentration of H_2O molecules in water that would be attained in the hypothetical case of water molecules occupying only the volume occupied by their atoms (i.e. n_{max} is the inverse of the volume that is occupied by the atoms of a water molecule or $n_{\text{max}} = (2v_{\text{hyd}} + v_{\text{oxy}})^{-1}$, where v_{hyd} and v_{oxy} (μm^3) are the atomic volumes of hydrogen and oxygen, respectively). Typical values are[12] $v_{\text{water}} = 0.02992$ x 10^{-9} μm^3 and $2v_{\text{hyd}} + v_{\text{oxy}} = 0.0146$ x 10^{-9} μm^3, which gives a ratio $\frac{n_{\text{water}}}{n_{\text{max}}} = \frac{2v_{\text{a,hyd}} + v_{\text{a,oxy}}}{v_{\text{water}}} \approx 0.49$, whereas a dense packing of spherical molecules would yield 0.74. Thus, a large part of the volume of liquid water is actually made of voids.

Then, using that $\mu_{\text{ice}} = \mu_{\text{s.water}}$ and Eqs. (2) and (3), we obtain that

$$kT_{\text{melt}}(x_s) = \frac{L_{\text{melt}} - \beta x_s}{\ln\left(\frac{n_{\text{max}}}{n_{\text{water}}}\right)}, \tag{4}$$

with $L_{\text{melt}} = \varepsilon_{\text{ice}} - \varepsilon_{\text{water}}$ being the latent heat of melting (eV per molecule). From this equation, we can obtain a more useful expression for the shift of the melting point:

$$\frac{T_{\text{melt}}(x_s)}{T_{\text{melt}}(0)} = \frac{L_{\text{melt}} - \beta\ x_s}{L_{\text{melt}}} = 1 - \frac{\beta x_s}{L_{\text{melt}}}. \tag{5}$$

This equation illustrates that the higher x_s, the lower $T_{\text{melt}}(x_s)$. In reality, once crystallisation/melting starts, x_s begins to change. In a crystallisation process it increases pushing $T_{\text{melt}}(x_s)$ down, which

eventually stops crystallisation. It looks like all the ice dissolved has now precipitated.

It is instructive to define x_s as a function of the volume concentration of dissolved ice

$$a_{\text{ice}} = \frac{V_{\text{ice}}}{V_{\text{s.water}} + V_{\text{ice}}}. \tag{6}$$

From here we have that

$$V_{\text{ice}} = \frac{a_{\text{ice}} V_{\text{s.water}}}{1 - a_{\text{ice}}} \tag{7}$$

and then

$$x_s(t) = \frac{M_s(1 - a_{\text{ice}}(t))}{V_{\text{s.water}}} = x_s(\bar{t})(1 - a_{\text{ice}}(t)), \tag{8}$$

where we recall that $\bar{t}$ (s) is the time when the maximum salt mass concentration is attained, which is achieved when all dissolved ice has precipitated. According to Eq. (5) we have

$$\frac{T_{\text{melt}}(x_s(\bar{t}))}{T_{\text{melt}}(0)} = 1 - \frac{\beta x_s(\bar{t})}{L_{\text{melt}}}.$$

Then, taking into account that $T_{\text{melt}}(x_s(\bar{t})) = T_{\text{exp}}$, we obtain

$$x_s(\bar{t}) = \frac{L_{\text{melt}}}{\beta}\left(1 - \frac{T_{\text{exp}}}{T_{\text{melt}}(0)}\right). \tag{9}$$

Let us suppose that, at the initial time t_0 the salt concentration is $x_s(t_0) = x_{s,0}$ and the volume of water plus dissolved ice is $V_{\text{s.water}} + V_{\text{ice}}(t_0) = V_0$. Then, we can find the amount of ice crystallised at temperature T_{exp}. From Eq. (1) we have

$$x_s(\bar{t}) = \frac{x_{s,0} V_0}{V_0 - V_{\text{ice}}(t_0)},$$

which implies that

$$V_{\text{ice}}(t_0) = V_0\left(1 - \frac{x_{s,0}}{x_s(\bar{t})}\right).$$

Then, from Eq. (6) we deduce that

$$a_{\rm ice}(t_0) = \frac{V_{\rm ice}(t_0)}{V_0} = 1 - \frac{x_{s,0}}{x_s(\bar{t})}. \tag{10}$$

Substituting Eq. (9) into Eq. (10) we obtain

$$a_{\rm ice}(t_0) = 1 - \frac{x_{s,0}}{\frac{L_{\rm melt}}{\beta}\left(1 - \frac{T_{\rm exp}}{T_{\rm melt}(0)}\right)} = 1 - \frac{\beta x_{s,0}}{L_{\rm melt}} \frac{T_{\rm melt}(0)}{(T_{\rm melt}(0) - T_{\rm exp})}. \tag{11}$$

We can also find the salt mass concentration at any time, as a function of the corresponding volume concentration of dissolved ice, by using the following expression, deduced from Eqs. (8) and (10)

$$x_s(t) = x_s(\bar{t})(1 - a_{\rm ice}(t)) = \frac{x_{s,0}(1 - a_{\rm ice}(t))}{1 - a_{\rm ice}(t_0)}. \tag{12}$$

3 Growth and ripening

Here we use the idea about dissolved ice in the water and find equations describing growth and ripening of pre-existing ice particles. For simplicity we assume that all the particles have spherical shape and retain it during the whole process. In the mean field theory of ordinary Ostwald ripening (OR)[7–9] the conservation of fluxes (total incoming and outgoing) is normally assumed. If there is supersaturation of one component (ice) in the other (water) such conservation does not take place anymore, i.e., the total particles mass increases. The equations for particle radii R (μm) in the Wagner limit[9] are

$$\frac{{\rm d}R}{{\rm d}t} = v_{\rm ice}\left(I_{\rm in} - I_{\rm out}(R)\right), \tag{13}$$

where $v_{\rm ice}$ (μm^3 per molecule) is the molecular volume of an H_2O molecule in ice and $I_{\rm in}$ and $I_{\rm out}$ (molecules per μm^2 and per s) are the densities of incoming and outgoing molecular fluxes, respectively. The latter can be written as

$$I_{\rm in} = K\, n_{\rm mf}, \quad I_{\rm out}(R) = K\, n_{\rm GT}(R),$$

where n_{mf} (ice molecules per $\mu\mathrm{m}^3$) is the mean field number concentration of dissolved ice, $n_{\mathrm{GT}}(R)$ is the Gibbs–Thomson number concentration and K ($\mu\mathrm{m\ s}^{-1}$) is the surface reaction rate.

It is convenient to represent the mean field concentration as a sum

$$n_{\mathrm{mf}} = n_{\mathrm{OR}} + n_{\mathrm{ice}}, \tag{14}$$

where the component n_{OR} (molecules per $\mu\mathrm{m}^3$) accounts for the dissolved ice concentration at which the total mass of the precipitated ice is conserved, and n_{ice} is the excess concentration of the dissolved ice accounting for the growth of that mass.

3.1 Ripening

The ice concentration component n_{OR} can be obtained according to its definition, i.e., from the balance of all emitted and absorbed molecular fluxes. The number of ice molecules deposited on an ice particle of radius R per unit time is $4\pi R^2 \left(I_{\mathrm{in}} - I_{\mathrm{out}}(R)\right)$. Therefore, taking into account all particles and assuming that the total number of ice molecules in all particles is conserved, we have

$$\sum_i R_i^2 \left(n_{\mathrm{OR}} - n_{\mathrm{GT}}(R_i)\right) = 0,$$

which implies, using mean values, that

$$n_{\mathrm{OR}} = \frac{\left\langle R^2\, n_{\mathrm{GT}}(R)\right\rangle}{\left\langle R^2\right\rangle}. \tag{15}$$

The Gibbs-Thomson concentration entering Eq. (13) by definition can be determined using the thermodynamic equilibrium condition between ice particle and salty water. Chemical potential ($\mu_{\mathrm{cl}}(R)$) of water molecule in the ice cluster is

$$\mu_{\mathrm{cl}}(R) = -\varepsilon_{\mathrm{ice}} + \frac{2\gamma v_{\mathrm{ice}}}{R}, \tag{16}$$

where γ is the cluster surface energy per unit area. The corresponding chemical potential in salty water is given by Eq. (3). In equilibrium $\mu_{\rm cl} = \mu_{\rm water}$ and from Eqs. (3), (12) and (16), it follows that

$$-\varepsilon_{\rm ice} + \frac{2\gamma v_{\rm ice}}{R(t)} = -\varepsilon_{\rm water} + kT_{\rm exp} \ln\left(\frac{n_{\rm GT}(t)}{n_{\rm max}}\right) - \frac{\beta x_{s,0}(1-a_{\rm ice}(t))}{1-a_{\rm ice}(0)}.$$

From this we obtain

$$n_{\rm GT}(R(t)) = n_{\rm max} \exp\left[-\frac{L_{\rm melt} - \frac{\beta x_{s,0}(1-a_{\rm ice}(t))}{1-a_{\rm ice}(0)}}{kT_{\rm exp}} + \frac{2\gamma v_{\rm ice}}{kT_{\rm exp}R(t)}\right]. \tag{17}$$

Using the usual approximation[13]

$$2\gamma v_{\rm ice} << kT_{\rm exp}R(t), \tag{18}$$

Eq. (17) can be simplified to obtain

$$n_{\rm GT}(R(t)) \approx n_{\rm max} \exp\left[-\frac{L_{\rm melt} - \frac{\beta x_{s,0}(1-a_{\rm ice}(t))}{1-a_{\rm ice}(0)}}{kT_{\rm exp}}\right]\left(1 + \frac{2\gamma v_{\rm ice}}{kT_{\rm exp}R(t)}\right). \tag{19}$$

Substituting Eq. (19) into Eq. (15) we find

$$n_{\rm OR} \approx n_{\rm max} \exp\left[-\frac{L_{\rm melt} - \frac{\beta x_{s,0}(1-a_{\rm ice}(t))}{1-a_{\rm ice}(0)}}{kT_{\rm exp}}\right]\left(1 + \frac{2\gamma v_{\rm ice}\langle R(t)\rangle}{kT_{\rm exp}\langle R(t)^2\rangle}\right). \tag{20}$$

3.2 Growth

The growth fraction $n_{\rm ice} = a_{\rm ice} v_{\rm ice}^{-1}$ of the mean field given in Eq. (14) can be determined from a separate equation. It is clear that

$$\mathrm{d}V_{\rm ice} = -\mathrm{d}\left(\sum_i \frac{4\pi}{3} R_i^3\right) = -\sum_i 4\pi R_i^2 \mathrm{d}R_i,$$

which implies that

$$\frac{\mathrm{d}V_{\rm ice}}{\mathrm{d}t} = -\sum_i 4\pi R_i^2 \frac{\mathrm{d}R_i}{\mathrm{d}t}.$$

Then, using Eq. (13) but accounting only for growth and without ripening (i.e. with $I_{\text{out}} = 0$ and $n_{\text{OR}} = 0$) we find the following equation for $V_{\text{ice}}(t)$

$$\frac{\mathrm{d}V_{\text{ice}}}{\mathrm{d}t} = -v_{\text{ice}} K n_{\text{ice}} \sum_i 4\pi R_i^2. \tag{21}$$

Let us now rewrite Eq. (21) in terms of a_{ice}. From Eqs. (7) and (10) we obtain

$$\frac{\mathrm{d}}{\mathrm{d}t}\left(\frac{a_{\text{ice}} V_0 (1 - a_{\text{ice}}(t_0))}{1 - a_{\text{ice}}}\right) = -v_{\text{ice}} K n_{\text{ice}} \sum_i 4\pi R_i^2 = -K a_{\text{ice}} \sum_i 4\pi R_i^2$$

$$\implies \qquad \frac{\mathrm{d}a_{\text{ice}}}{\mathrm{d}t}\left(\frac{1}{1 - a_{\text{ice}}} + \frac{a_{\text{ice}}}{(1 - a_{\text{ice}})^2}\right) = -\frac{K a_{\text{ice}}}{V_0 (1 - a_{\text{ice}}(t_0))} \sum_i 4\pi R_i^2. \tag{22}$$

3.3 Ripening and growth

The full set of equations is then obtained from Eqs. (19), (20) and (22)

$$\begin{cases} \dfrac{\mathrm{d}a_{\text{ice}}(t)}{\mathrm{d}t} = -\dfrac{K a_{\text{ice}}(t)(1 - a_{\text{ice}}(t))^2}{V_0 (1 - a_{\text{ice}}(t_0))} \displaystyle\sum_i 4\pi R_i(t)^2 \\ \dfrac{\mathrm{d}R_i(t)}{\mathrm{d}t} = K a_{\text{ice}}(t) + \dfrac{2\gamma v_{\text{ice}}^2 K n_{\max}}{k T_{\text{exp}}} \exp\left[-\dfrac{L_{\text{melt}}}{k T_{\text{exp}}} + \dfrac{\beta x_{s,0}(1 - a_{\text{ice}}(t))}{k T_{\text{exp}}(1 - a_{\text{ice}}(t_0))}\right]\left(\dfrac{\langle R(t)\rangle}{\langle R(t)^2\rangle} - \dfrac{1}{R_i(t)}\right). \end{cases}$$

Parameter $n_{\max}$ can be eliminated from the above equation recalling that (see Eq. (4)),

$$n_{\max} = n_{\text{water}} \exp\left(\frac{L_{\text{melt}}}{k T_{\text{melt}}(0)}\right).$$

Thus, the system can be written as

$$\begin{cases} \dfrac{\mathrm{d}a_{\text{ice}}(t)}{\mathrm{d}t} = -\dfrac{K a_{\text{ice}}(t)(1 - a_{\text{ice}}(t))^2}{V_0 (1 - a_{\text{ice}}(t_0))} \displaystyle\sum_i 4\pi R_i(t)^2 \\ \dfrac{\mathrm{d}R_i(t)}{\mathrm{d}t} = K a_{\text{ice}}(t) + \\ \qquad \dfrac{2\gamma v_{\text{ice}}^2 v_{\text{water}}^{-1} K}{k T_{\text{exp}}} \exp\left[\dfrac{L_{\text{melt}}}{k}\left(\dfrac{1}{T_{\text{melt}}(0)} - \dfrac{1}{T_{\text{exp}}}\right) + \dfrac{\beta x_{s,0}(1 - a_{\text{ice}}(t))}{k T_{\text{exp}}(1 - a_{\text{ice}}(t_0))}\right]\left(\dfrac{\langle R(t)\rangle}{\langle R(t)^2\rangle} - \dfrac{1}{R_i(t)}\right). \end{cases} \tag{23}$$

This system must be completed with initial conditions at a suitable time t_0 (s). The initial ice volume concentration $a_{\text{ice}}(t_0)$ is calculated using Eq. (11). $R_i(0)$ and the number of index i have to be estimated from experiments

$$\begin{cases} a_{\text{ice}}(t_0) = 1 - \dfrac{\beta x_{s,0}}{L_{\text{melt}}} \dfrac{T_{\text{melt}}(0)}{(T_{\text{melt}}(0) - T_{\text{exp}})}, \\ R_i(t_0) \text{ estimated from experiments.} \end{cases} \tag{24}$$

Eqs. (23) and (24) are solved numerically to obtain time evolution of the ice particle radii and dissolved ice concentration.

4 Numerical simulations

4.1 Estimation of some parameters for simulations

The model described by Eqs. (23) and (24) needs the value of the well–known constants (which we give in the relevant units for this paper) $k \approx 8.617$ x 10^{-5} (eV K^{-1}), $T_{\text{melt}}(0) \approx 273.15$ (K), $L_{\text{melt}} \approx 0.0625$ (eV molecule^{-1}), $\gamma \approx 1.5605$ x 10^5 (eV μm^{-2}), $v_{\text{water}} \approx 0.02992$ x 10^{-9} (μm^3) and $v_{\text{ice}} \approx 0.03263\ 10^{-9}$ (μm^3). It also needs the following input parameters: T_{exp}, K, V_0, β, $x_{s,0}$ and $R_i(0)$, for all i.

Now,

$$\frac{2\gamma v_{\text{ice}}^2 v_{\text{water}}^{-1}}{k} \approx \frac{2 \cdot 1.5605 \cdot 10^5 \cdot 0.03263^2 \cdot 10^{-18}}{0.02992 \cdot 10^{-9} \cdot 8.617 \cdot 10^{-5}} \approx 0.12887\ \mu\text{m K},$$

$$\frac{L_{\text{melt}}}{k} \approx \frac{0.0625}{8.617 \cdot 10^{-5}}\ \text{K molecule}^{-1} \approx 725.31\ \text{K molecule}^{-1},$$

$$\frac{L_{\text{melt}}}{kT_{\text{melt}}(0)} \approx \frac{725.31}{273.15}\ \text{molecule}^{-1} \approx 2.6554\ \text{molecule}^{-1},$$

$$\frac{1}{k} = \frac{1}{8.617 \cdot 10^{-5}}\ \text{K eV}^{-1} \approx 11604.967\ \text{K eV}^{-1},$$

and

$$\frac{T_{\text{melt}}(0)}{L_{\text{melt}}} \approx \frac{273.15}{0.0625} = \approx 4370.4\ \text{K eV}^{-1}\ \text{molecule}.$$

Therefore, Eq. (23) can be approximated for the simulations by

$$\begin{cases} \dfrac{\mathrm{d}a_{\mathrm{ice}}(t)}{\mathrm{d}t} = C_{a_{\mathrm{ice}}}(t) \\ \dfrac{\mathrm{d}R_i(t)}{\mathrm{d}t} = C_{R_i}(t), \end{cases} \tag{25}$$

where

$$\begin{cases} C_{a_{\mathrm{ice}}}(t) = -\dfrac{K a_{\mathrm{ice}}(t)(1-a_{\mathrm{ice}}(t))^2}{V_0(1-a_{\mathrm{ice}}(t_0))} \displaystyle\sum_i 4\pi R_i(t)^2 \\ C_{R_i}(t) = K a_{\mathrm{ice}}(t) + \\ \qquad 0.12887 \dfrac{K}{T_{\mathrm{exp}}} \exp\left[2.6554 - \dfrac{725.31}{T_{\mathrm{exp}}} + 11604.967 \dfrac{\beta x_{s,0}(1-a_{\mathrm{ice}}(t))}{T_{\mathrm{exp}}(1-a_{\mathrm{ice}}(t_0))}\right] \left(\dfrac{\langle R_i(t)\rangle}{\langle R(t)^2\rangle} - \dfrac{1}{R_i(t)}\right). \end{cases} \tag{26}$$

The initial conditions given in Eq. (24) can be approximated by

$$\begin{cases} a_{\mathrm{ice}}(t_0) = 1 - 4370.4 \dfrac{\beta x_{s,0}}{(273.15 - T_{\mathrm{exp}})}, \\ R_i(t_0) \text{ estimated from experiments.} \end{cases} \tag{27}$$

The rest of the input parameters have to be given in the following units: T_{exp} (K), K (μm s^{-1}), V_0 (μm^3), β (eV μm^3 mg^{-1} per molecule) $x_{s,0}$ (mg μm^{-3}) and $R_i(0)$ (μm), for all i.

4.2 Numerical approximation

The numerical model was implemented in Fortran using a first-order explicit Euler scheme. The estimation of parameters described in Section 4.1 was used in the numerical algorithm. Time was discretised from the initial time, t_0, to final time, t_{f}, using a step $\mathrm{d}t$. The numerical scheme was initiated using Eq. (27) and at a given time t, if we know $a_{\mathrm{ice}}(t)$ and $R_i(t)$ we calculate those values at the following time step as

$$\begin{cases} a_{\mathrm{ice}}(t+\mathrm{d}t) = a_{\mathrm{ice}}(t) + \mathrm{d}t \cdot C_{a_{\mathrm{ice}}}(t) \\ R_i(t+\mathrm{d}t) = R_i(t) + \mathrm{d}t \cdot C_{R_i}(t), \end{cases} \tag{28}$$

with $C_{a_{\text{ice}}}(t)$ and $C_{R_i}(t)$ given by Eq. (26).

In analogy with Burlakov and Kantorovich,[13] an ice particle with the size below a certain threshold value R_{thr} is declared as dissolved with its residual content being transferred to other particles in proportion to their surface area. For our simulations we have considered $R_{\text{thr}} = 0.01$ μm.

5 Simulation results

We set up two different numerical experiments to validate our model. For the first one we use experimental data from Fernández et al.[6], where a salty water solution as a food model was used. Our model is designed specifically for salty water, and we show below that the experimental data fit very well. The second model validation is done using ice-cream as a food model and is based on published work.[14] Even though ice cream is a much more complex system than salty water, we adjust the model to this case, and we see reasonable agreement.

5.1 Salty water food model

Fernández et al.[6] used a 1.86N NaCl solution as a food model. The concentration was selected such that at the HPSF recrystallisation temperature (approximately -19.2°C) the frozen fraction was approximately 51%. Temperature was raised from -19.2°C to the target experimental temperature and kept constant for a period of 3 h to study recrystallisation phenomena. The authors consider this time period long enough to represent the more intense phase of the recrystallisation process. These target experimental temperatures were -19.2°C for comparison of HPSF and APF frozen samples (which we refer to as HPSF -19.2 and APF -19.2) and -14.3°C, -12.4°C, -9.5°C (which we refer to as APF -14.3, APF -12.4 and APF -9.5, respectively) for system temperature dependence study. The evolution of the ice crystals during this period was followed by micrographs that were automatically taken every 30 minutes. An image analysis software was used to detect crystal boundaries from the micrographs, and from this a diameter for each crystal was determined.

5.1.1 Discrete experimental data

The data we have available are the radii of the crystals at each time step. Figure 2 shows the maximum and mean radius evolution for each of the experiments. We would like to remark that the maximum radii data are not very reliable, as they should generate a monotonic increasing function over time, and as can be seen for some cases it is not. We think this is due to the fact that in the experimental observations a very small sample was analysed,[6] which meant that on average there were 150-200 initial crystals, not enough to get more accurate results. The mean radii evolution, however, looks more reliable.

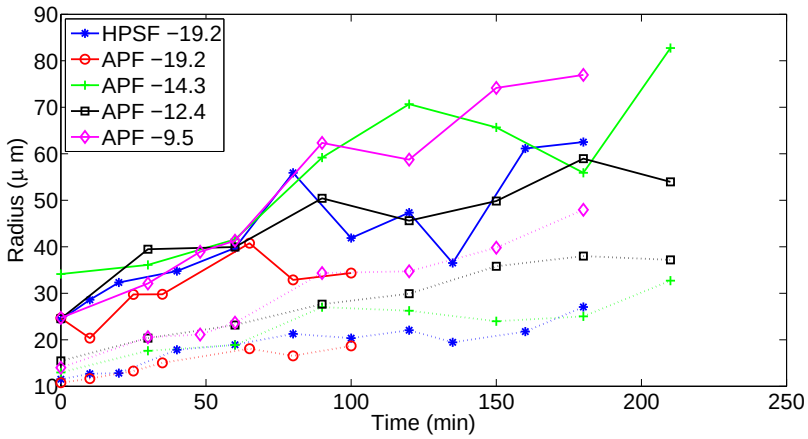

Figure 2: Mean (dotted lines) and maximum (solid lines) experimental ice particle radius values for salty water data

For simulating the same experiments with our model we consider the input parameters V_0, $R_i(t_0)$, T_{exp}, K, β and $x_{s,0}$ (see Section 4.1). From the experimental data we have the size distribution of ice particles $R_i(t_0)$ (in μm) at the temperature T_{exp}=-19.2°C (253.95 K) where the frozen fraction of the solution was approximately 51%.[6] The initial volume of the sample V_0 (μm^3) is taken for each case according to the following procedure: we assume that the initial amount of frozen ice (nucleated) is 16% and that the final amount of frozen ice is approximately 51% (i.e. for each experiment there is a total ice fraction of 0.51 and a dissolved ice fraction of 0.35). Then we choose the total number of particles suitable for simulations and choose the total system volume to fit the ice fraction given. For each experiment the number of particles and volumes are different,

and are pointed out separately in each graph (see Figures 3 and 4). The initial salt mass concentration, $x_{s,0}$, is calculated according to the fact that we use a 1.86 N NaCl solution. By converting normality to solute mass concentration in the relevant units, we get $x_{s,0} = 1.0881 \cdot 10^{-10}$ mg μm^{-3}. Finally, K and β are model fitting parameters. For all of the salty water experiments we take $K = 1$ μm s^{-1} and $\beta = 2.757 \cdot 10^{7}$ eV μm^4 mg^{-1} molecule^{-1}.

Let us see, for the case under study, if inequality Eq. (18) holds. As $k \approx 8.617$ x 10^{-5} (eV K^{-1}), $T_{\text{exp}} = 253.95$ (K), $\gamma \approx 1.5605$ x 10^5 (eV μm^{-2}) and $v_{\text{ice}} \approx 0.03263$ 10^{-9} (μm^3), we have that for Eq. (18) to hold, necessarily,

$$R_i >> \frac{2\gamma v_{\text{ice}}}{kT_{\text{exp}}} = 4.6538 \text{ x } 10^{-4} \ \mu\text{m}, \ \forall i,$$

which is true given that all particles in the model have a larger radius than the threshold one (otherwise they disappear) and $R_{\text{thr}} = 0.01$ μm.

As mentioned previously, the experimental data have been recorded for 3 h with the data points taken every 30 minutes. We run simulations for much longer times to obtain the long term behaviour of the particle size distribution. On a shorter time scale this behaviour is compared to that obtained experimentally. According to Fernández et al.[6] the size distribution significantly changes with storage time for both the HPSF and APF models. As the experimental size distributions are rather sparse, they cannot be properly compared to the simulated ones. More relevant characteristics to assess the quality of modelling approach are average and maximum particle sizes.

Figures 3a and 3b show the simulated and experimental time evolution of average and maximum particle sizes for HPSF -19.2 and the APF -19.2 processes, respectively. For both cases the simulated average radius matches the experimental average radius very well, and as can be seen we let the simulated radius evolve for longer than 3 h. In contrast, the simulated maximum radius does not show similarly good agreement with experimental data most likely due to the rather low number of measured particles. We find that the long term behaviour of the characteristic radii for the samples frozen using HPSF and APF are very similar in agreement with the results reported in

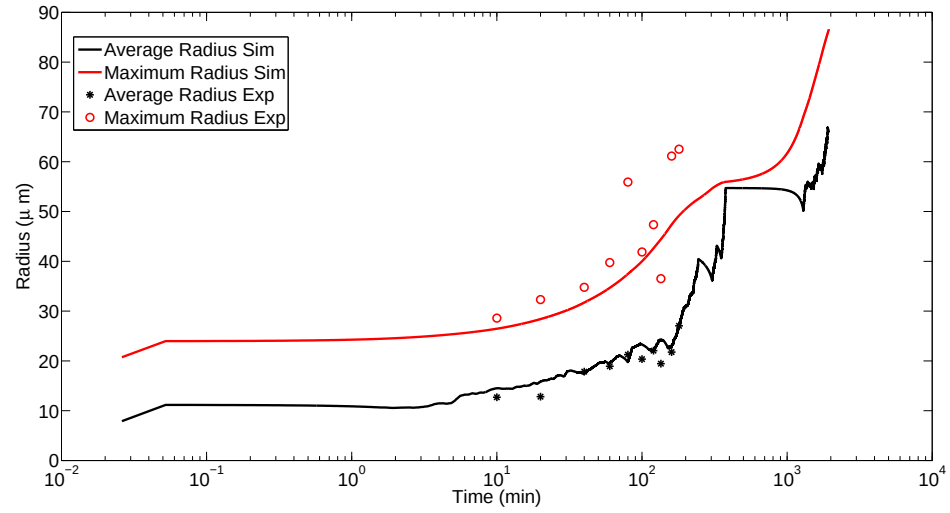

(a) HPSF -19.2 (Number of particles=8000; $V_0 = 1.05$ x 10^8 μm^3)

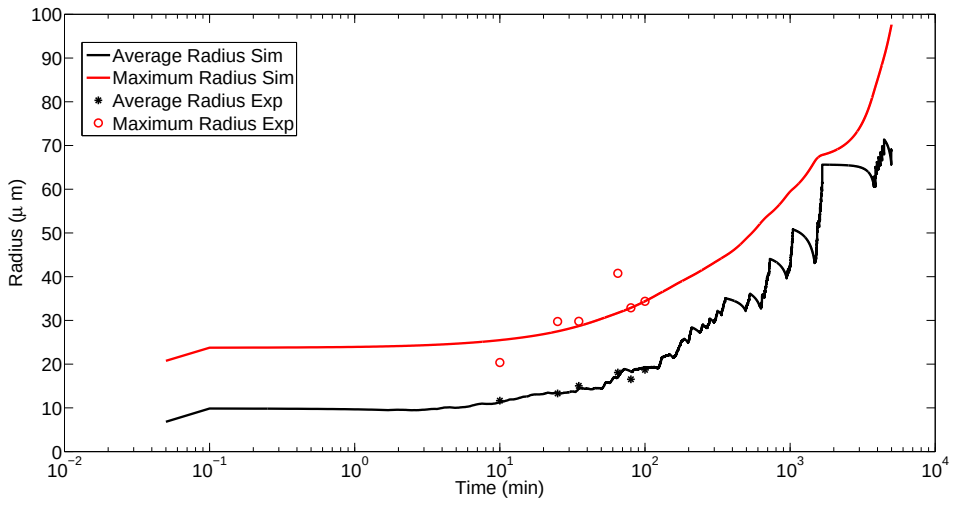

(b) APF -19.2 (Number of particles=5000; $V_0 = 4.8$ x 10^7 μm^3)

Figure 3: Experimental and simulated average and maximum ice particle radius evolution (in logarithmic scale) for salty water experiment

Fernández et al.[6]. Note that the simulated radii evolution curves are not smooth due to the relatively low number of particles used in the simulations. This is especially evident as the number of particles decreases with time due to dissolution of smaller particles.

Figures 4a to 4c show the simulated and experimental radii evolution over time for the APF -14.3, APF -12.4 and the APF -9.5 processes. Once more the agreement between experimental and simulated average radii is rather good for all the processes. The oscillations observed in the simulated curves are again due to the low and decreasing number of ice particles. As we will see in Section 5.1.2 such oscillations disappear if the number of particles is high enough making the initial distribution very smooth.

5.1.2 Continuous experimental data

To test the validity of our model for predicting ice crystal size distributions at a given time we design a new set of data from experiment APF -12.4 described in Section 5.1.1. A continuous (large number of particles) initial distribution is generated using the values of the average particle radius and standard deviation obtained from the discrete experimental size distribution approximated with the normal distribution. Figure 5 shows the distributions (Figure 5a) and the average and maximum simulated and experimental radii time evolution (Figure 5b). Again the average radii match very well and the simulated radii curves are now much smoother than in the discrete case (see Figure 4b), due to the smoothness of the continuous initial distribution.

5.2 Ice-cream food model

Our second numerical experiment uses ice-cream as a food model. As previously stated, ice-cream is a much more complex system than salty water and it is instructive to try our model with the ice-cream to see if the experimental results can be fitted. In Donhowe et al.[14] a methodology to characterise the ice crystal size distribution was developed and several ice-cream and ice milk formulations of various composition were analysed to test the methodology. We use the 40% total solids (TS) ice-cream formulation, as the experimental data are available for this particular com-

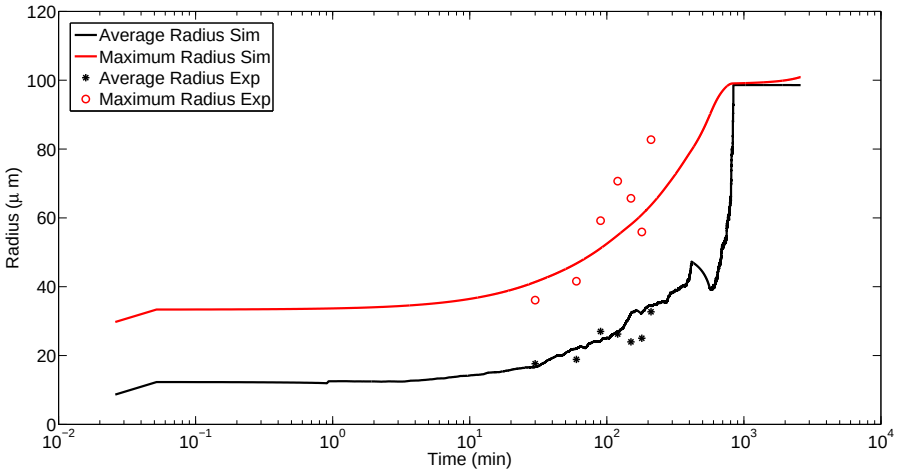

(a) APF -14.3 (Number of particles=10000; $V_0 = 1.8$ x 10^8 μm^3)

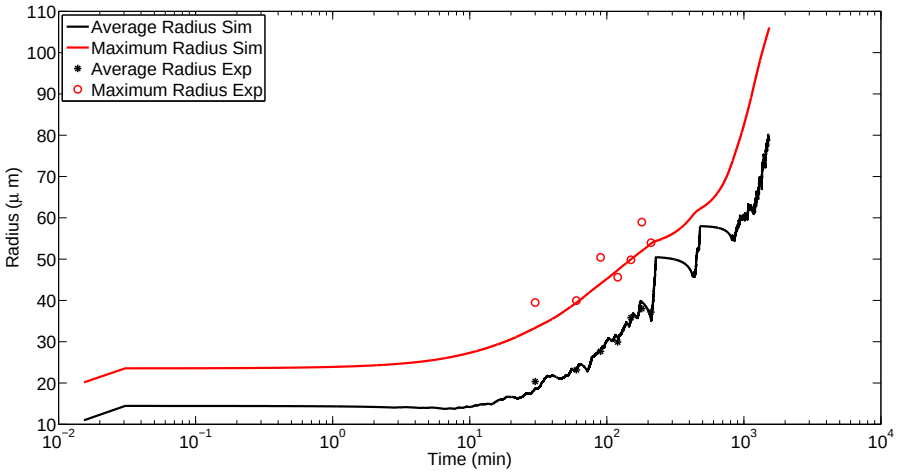

(b) APF -12.4 (Number of particles=5000; $V_0 = 1.05$ x 10^8 μm^3)

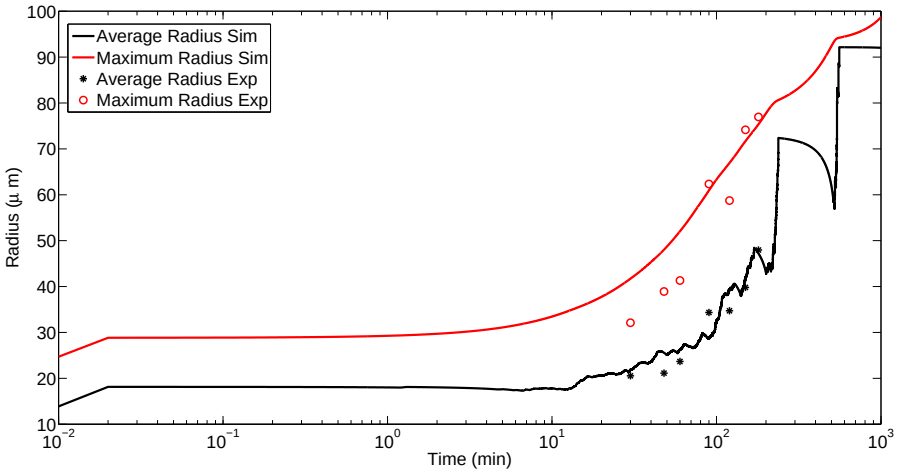

(c) APF -9.5 (Number of particles=10000; $V_0 = 4$ x 10^8 μm^3)

Figure 4: Experimental and simulated average and maximum ice particle radius evolution (in logarithmic scale) for salty water experiment

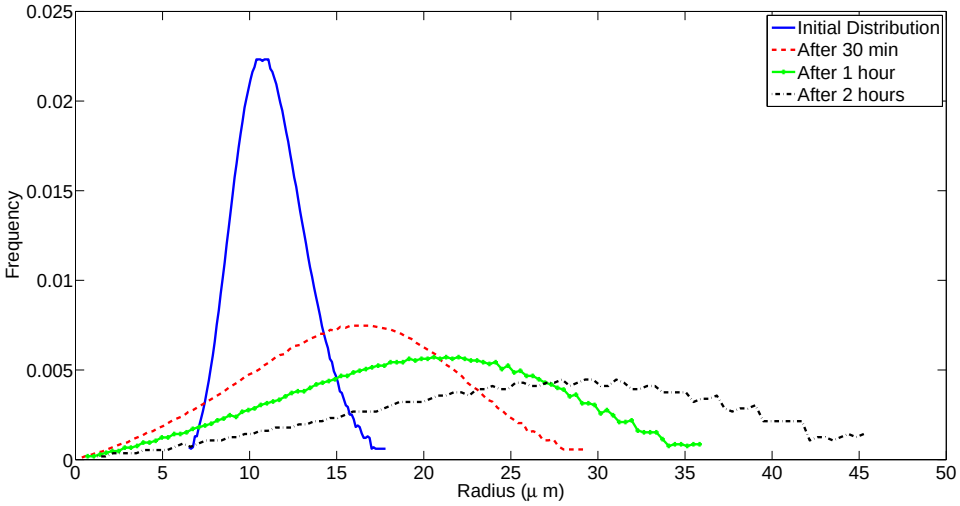

(a) Ice particle distributions

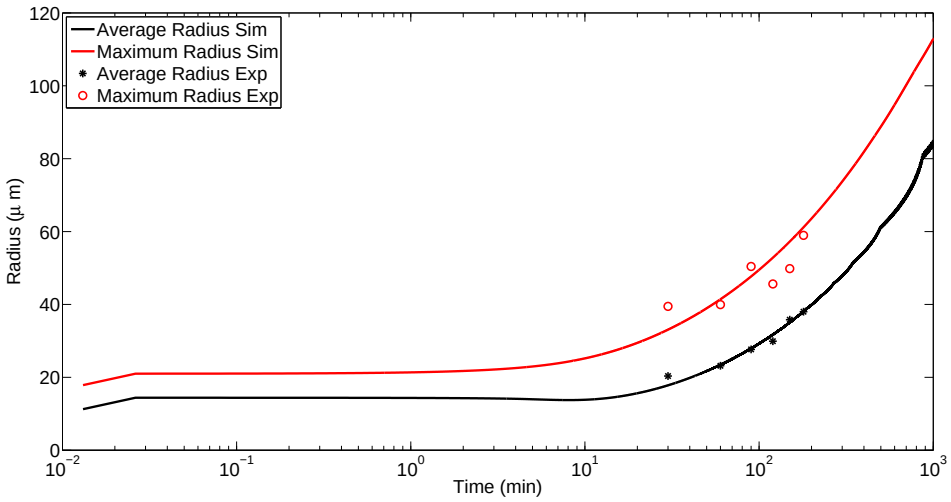

(b) Ice particle radius evolution (in logarithmic scale)

Figure 5: APF $-12.4°$C Continuous model (Number of particles=12000; $V_0 = 2.2$ x 10^8 μm^3)

position.[14] In the experiment the samples were frozen, then drawn from the freezer and hardened for 24 h, and finally stored in a storage freezer for several weeks. The samples were analysed for crystal size distribution immediately after drawing from the freezer (the temperature was set to the draw temperature, -7.3 ± 0.3°C); after hardening (at -14°C) and then after 7 and 14 weeks of storage (also at -14°C). To set up the numerical experiment within our model the following assumptions are made: we consider all time evolution to take place at one and the same temperature $T_{\text{exp}} = -14$°C (259.15 K). All experimental measurements except for the one immediately after drawing from the freezer have been taken at this temperature. Because of the differences in temperature between the drawing and hardening stages, a significant increase in the ice particle size was observed.[14] Our model does not account for this temperature difference but it still accounts for the ice particle growth due to ripening. The initial size distribution, $R_i(t_0)$, is obtained using Figure 4 from Donhowe et al.[14] where we extrapolate the published curve and create a histogram, which is then used for generation of initial distribution in our simulations. We take the initial amount of ice formed after drawing to be approximately 25%, and the dissolved ice concentration of the same amount, giving the total ice fraction of 50%. For obtaining smooth distributions we consider quite a large number of particles, 4500, and therefore the system volume is taken as $1.2{\cdot}10^9$ μm^3, to get the correct ice fractions. In this case we do not have a value for $x_{s,0}$ from the experimental data, as we are no longer working with salty water but with ice-cream instead, which has many more components. The latter means that there are now three fitting parameters, β, $x_{s,0}$ and K. As the first two parameters are involved as a product, they can be replaced with just one fitting parameter. Thus, we take $\beta x_{s,0} = 0.0024$ eV molecule^{-1}, which is very close to the value used for the salty water $\beta x_{s,0} = 0.003$ eV molecule^{-1}. For K we stick to the same value as for the salty water experiments, i.e. $K = 1$ μm s^{-1}.

Again for this case, inequality Eq. (18) holds. The only parameter that has changed with respect to the salty water model is T_{exp} which is now 259.15 K, leading to

$$R_i >> 4.5604 \text{ x } 10^{-4} \ \mu\text{m}, \ \forall i,$$

which is true given $R_{\text{thr}} = 0.01\ \mu$m.

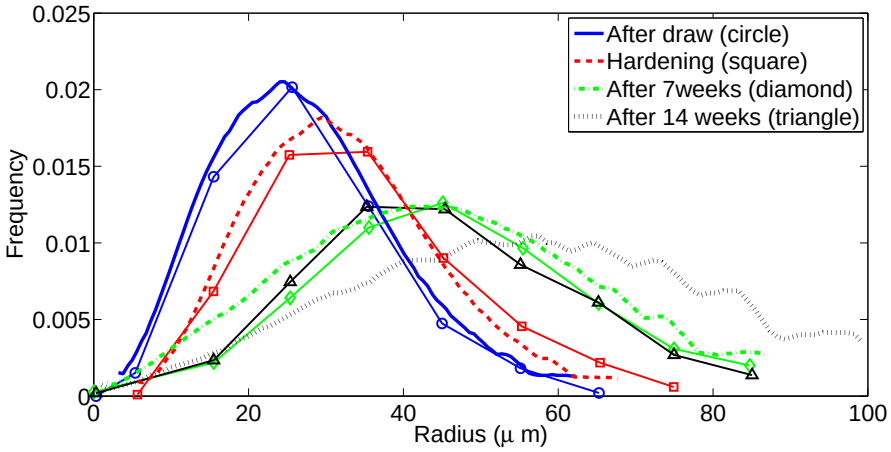

(a) Simulated (lines) and experimental (lines with symbols) ice particle distributions

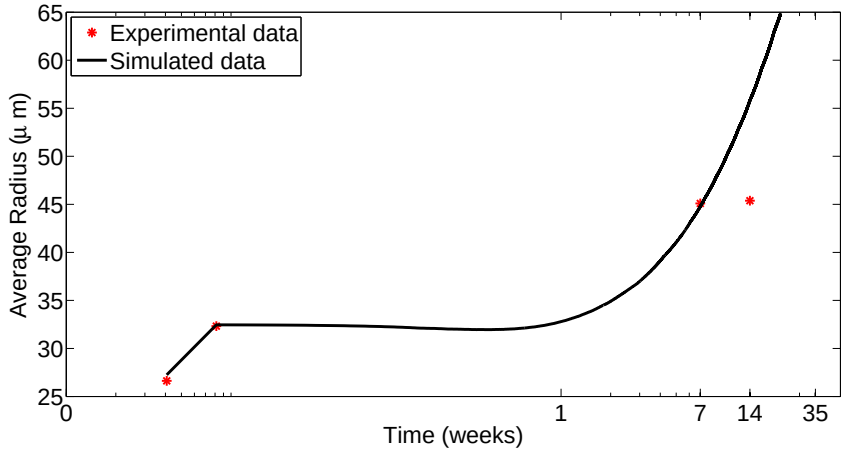

(b) Ice particle radius evolution (in logarithmic scale)

Figure 6: Ice-cream model

Figure 6 shows the simulated (lines) and experimental (lines with symbols) distributions (Figure 6a) and the average and maximum simulated and experimental radius evolution over time (Figure 6b). The model prediction for the size distribution agrees well with the experimental data except for the those taken after 14 weeks when the experimental ice particles have stopped coarsening (the 7 weeks and 14 weeks distributions are practically the same), whereas the simulated ones continue to coarsen. We believe that this effect is due to the fact that ice-cream contains fat and emulsifiers which provide mechanical obstructions to the exchange of water molecules between ice particles,[14] something that our model does not account for.

6 Conclusions

We develop a very simple but powerful model that allows simulating growth and coarsening of ice crystals. Comparison of modelling results with those obtained experimentally is done for two food model systems: salty water and ice-cream. The model is accurate enough to correctly predict the time evolution of average ice crystal size for all cases. It also predicts rather well the evolution of crystal size distribution when continuous initial size distribution is available. The model allows reasonably accurate estimation of food storage time using certain criteria for acceptable ice particle size. Further development of the described model can be made by considering more complicated multi-component system including components acting as surfactants, and by allowing the temperature variation during the system time evolution.

Acknowledgement

This work was carried out thanks to the financial support of the Spanish "Ministry of Economy and Competitiveness" under projects MTM2008-04621 and MTM2011-22658; the "Fundación Caja Madrid"; and the "Comunidad de Madrid" and "European Social Fund" through project S2009/PPQ-1551. This publication was also based on work supported in part by Award No KUK-C1-013-04, made by King Abdullah University of Science and Technology (KAUST).

References

(1) Fernández, P. P.; Otero, L.; Guignon, B.; Sanz, P. D. *Food Hydrocolloids* **2006**, *20*, 510–522.

(2) Otero, L.; Sanz, P. D. *Biotechnol. Prog.* **2000**, *16*, 1030–1036.

(3) Otero, L.; Sanz, P. D. *J. Food Engng* **2006**, *72*, 354–363.

(4) Sanz, P. D.; Otero, L. *Biotechnol. Prog.* **2000**, *16*, 1037–1043.

(5) Smith, N. A. S.; Peppin, S. S. L.; Ramos, A. M. *Proc. Roy. Soc. A* **2012**, *468*, 2744–2766.

(6) Fernández, P. P.; Otero, L.; Martino, M. M.; Molina-García, A. D.; Sanz, P. D. *European Food Research and Technology* **2008**, *227*, 1367–1377.

(7) Lifshitz, I. M.; Slyozov, V. V. *Zh. Eksp. Teor. Fiz.* **1958**, *35*, .

(8) Lifshitz, I. M.; Slyozov, V. V. *J. Phys. Chem. Solids* **1961**, *19*, .

(9) Wagner, C. Z. *Electrochem.* **1961**, *65*, .

(10) Becker, B. R.; Fricke, B. A. *Int. Comm. Heat Mass Transfer* **1999**, *26*, 627–636.

(11) Job, G.; Herrmann, F. *European Journal of Physics* **2006**, *27*, 353–371.

(12) Cabane, B.; Vuilleumier, R. *C. R. Geoscience* **2005**, *337*, 159–171.

(13) Burlakov, V. M.; Kantorovich, L. *The Journal of Chemical Physics* **2011**, *134*, 024521.

(14) Donhowe, D. P.; Hartel, R. W.; R. L. Bradley, J. *J. Dairy Sci.* **1991**, *74*, 3334–3344.

PREPUBLICACIONES DEL DEPARTAMENTO
DE MATEMÁTICA APLICADA
UNIVERSIDAD COMPLUTENSE DE MADRID
MA-UCM 2012

1. ON THE CAHN-HILLIARD EQUATION IN H^1(R^N), J. Cholewa and A. Rodríguez Bernal

2. GENERALIZED ENTHALPY MODEL OF A HIGH PRESSURE SHIFT FREEZING PROCESS, N. A. S. Smith, S. S. L. Peppin and A. M. Ramos

3. 2D AND 3D MODELING AND OPTIMIZATION FOR THE DESIGN OF A FAST HYDRODYNAMIC FOCUSING MICROFLUIDIC MIXER, B. Ivorra, J. L. Redondo, J. G. Santiago, P.M. Ortigosa and A. M. Ramos

4. SMOOTHING AND PERTURBATION FOR SOME FOURTH ORDER LINEAR PARABOLIC EQUATIONS IN R^N, C. Quesada and A. Rodríguez-Bernal

5. NONLINEAR BALANCE AND ASYMPTOTIC BEHAVIOR OF SUPERCRITICAL REACTION-DIFFUSION EQUATIONS WITH NONLINEAR BOUNDARY CONDITIONS, A. Rodríguez-Bernal and A. Vidal-López

6. NAVIGATION IN TIME-EVOLVING ENVIRONMENTS BASED ON COMPACT INTERNAL REPRESENTATION: EXPERIMENTAL MODEL, J. A. Villacorta-Atienza and V.A. Makarov

7. ARBITRAGE CONDITIONS WITH NO SHORT SELLING, G. E. Oleaga

8. THEORY OF INTERMITTENCY APPLIED TO CLASSICAL PATHOLOGICAL CASES, E. del Rio, S. Elaskar, and V. A. Makarov

9. ANALYSIS AND SIMPLIFICATION OF A MATHEMATICAL MODEL FOR HIGH-PRESSURE FOOD PROCESSES, N. A. S. Smith, S. L. Mitchell and A. M. Ramos

10. THE INFLUENCE OF SOURCES TERMS ON THE BOUNDARY BEHAVIOR OF THE LARGE SOLUTIONS OF QUASILINEAR ELLIPTIC EQUATIONS. THE POWER LIKE CASE, S.Alarcón, G.Díaz and J.M.Rey

11. SUSTAINED INCREASE OF SPONTANEOUS INPUT AND SPIKE TRANSFER IN THE CA3-CA1 PATHWAY FOLLOWING LONG TERM POTENTIATION IN VIVO, O. Herreras, V. Makarov and A. Fernández--Ruiz

12. ELLIPTIC EQUATIONS IN WEIGHTED BESOV SPACES ON ASYMPTOTICALLY FLAT RIEMANNIAN MANIFOLDS, U. Brauer and L. Karp

13. A NUMERICAL METHOD TO SOLVE A DUOPOLISTIC DIFFERENTIAL GAME IN A CLOSED-LOOP EQUILIBRIUM, J. H. de la Cruz, B.Ivorra and A. M. Ramos

14. EVALUATION OF THE RISK OF CLASSICAL SWINE FEVER SPREAD IN BULGARIA BY USING THE EPIDEMIOLOGICAL MODEL BE-FAST, B. Martínez-López. B.Ivorra, A. M. Ramos, E. Fernández, T. Alexandrov and J.M. Sánchez-Vizcaíno

15. WAVE-PROCESSING OF LONG-SCALE INFORMATION IN NEURONAL CHAINS, J. A. Villacorta-Atienza and V. A. Makarov

16. A NOTE ON THE EXISTENCE OF GLOBAL SOLUTIONS FOR REACTION-DIFFUSION EQUATIONS WITH ALMOST-MONOTONIC NONLINEARITIES, A. Rodríguez-Bernal and A. Vidal-López

PREPUBLICACIONES DEL DEPARTAMENTO
DE MATEMÁTICA APLICADA
UNIVERSIDAD COMPLUTENSE DE MADRID
MA-UCM 2013

1. THIN DOMAINS WITH DOUBLY OSCILLATORY BOUNDARY , J.M. Arrieta and M Villanueva-Pesqueira

2. ESTIMATES ON THE DISTANCE OF INERTIAL MANIFOLDS, J.M. Arrieta and E. Santamaría

3. A PRIORI BOUNDS FOR POSITIVE SOLUTIONS OF SUBCRITICAL ELLIPTIC EQUATIONS, A. Castro and R. Pardo

4. EVALUATION OF THE DIFFERENCES OF PROCESS VARIABLES IN VERTICAL AND HORIZONTAL CONFIGURATIONS OF HIGH PRESSURE THERMAL (HPT) PROCESSING SYSTEMS THROUGH NUMERICAL MODELLING, N. A. S. Smith, K. Knoerzer and A. M. Ramos

5. MATHEMATICAL MODELLING OF THE GROWTH AND COARSENING OF ICE PARTICLES IN THE CONTEXT OF HIGH PRESSURE SHIFT FREEZING PROCESSES, N. A. S. Smith, V. M. Burlakov and A. M. Ramos